

# Insights Into Thermal Runaway of Li–Ion Cells by Accelerating Rate Calorimetry Coupled with External Sensors and Online Gas Analysis

Abdelaziz A. Abd-El-Latif,<sup>[a]</sup> Peter Sichler,<sup>[a]</sup> Michael Kasper,<sup>[a]</sup> Thomas Waldmann,\*<sup>[a]</sup> and Margret Wohlfahrt-Mehrens<sup>[a]</sup>

Besides high energy density, fast-charging capability, and costs, safety of Li-ion batteries is fundamentally important – even after long-term usage or abusive conditions. In this paper, a new combination of accelerating rate calorimetry (ARC) coupled with a mass spectrometer (MS), as well as cell resistance and audio recording was applied to study commercial 18650-type Li-ion cells. This novel ARC-MS setup allows following the electrochemical and thermal behavior simultaneously to the evolved gases during cell venting and thermal runaway. The tested cells were (i) unaged, (ii) aged by low temperature cycling (main mechanism: Li deposition), as well as (iii) overcharged. The aged and the overcharged cells show an early onset-of-self-heating at 36 °C whereas the self-

heating started at 96 °C for the unaged cells. The rank of the time until explosion of the cells is in the order of overcharged cell < aged cell with Li deposition < unaged cell. The simultaneous recording of 13 individual values allows drawing conclusions on processes like separator pore closure, cell venting, explosion, and gas formation. Due to electrolyte decomposition by anodic and cathodic exothermic reactions, the amount of formed gases such as CO<sub>2</sub>, ethylene, and POF<sub>3</sub> are depending on the history of the cell, i.e., aging mechanism or overcharging. Additional gas sensors in the battery pack for improved battery safety are indicating venting of the cells and therefore might be a low cost solution.

## 1. Introduction

Nowadays, the demand for rechargeable lithium-ion batteries (LIBs) is constantly increasing in a variety of mobile and stationary applications, such as garden & power tools, smart phones, tablet computers, as well as hybrid electric vehicles (HEV) and battery electric vehicles (BEV).<sup>[1]</sup> Due to this high demand, optimization of the LIBs in terms of energy density, high power ability, lifetime, and fast charging is needed. Besides these challenges, safety has attracted attention due to cases of fire and explosion accidents in the last two decades.<sup>[2,3]</sup>

With rising temperatures, a variety of exothermic chemical reactions can occur between anode, cathode, and electrolyte, generating substantial heat inside the cells. If the heat transfer to the surroundings is not sufficient, the chemical reactions between the cell components accelerate. Cell leakage, venting, flames, and finally cell explosion can be the consequences. Classical accelerating rate calorimetry (ARC) experiments allow

to force LIBs into thermal runaway and observe their thermal behavior.

ARC and differential scanning calorimetry (DSC) were applied to measure the thermal response for high-power cells containing NCA cathodes by Roth and Doughty.<sup>[4]</sup> They reported three stages of heat formation.<sup>[4]</sup> The first stage is the decomposition of the solid-electrolyte interphase (SEI) layer between 100 and 120 °C followed by electrolyte decomposition reactions and finally the cathode reactions in the range of 200–250 °C.<sup>[4]</sup> The cathodic reactions showed a high rate of thermal runaway over a narrow temperature range (> 100 °C min<sup>-1</sup>) compared to the anodic reactions and a strong dependency on state-of-charge (SOC).<sup>[4]</sup> Abraham et al. analyzed the generated gases of 18650-type carbon/LiNi<sub>0.8</sub>Co<sub>0.15</sub>Al<sub>0.05</sub>O<sub>2</sub> cells collected after thermal runaway by gas chromatography/mass spectroscopy (GC-MS).<sup>[5]</sup> The major evolved gases were CO<sub>2</sub> and CO with a minor amount of H<sub>2</sub>, C<sub>2</sub>H<sub>4</sub>, CH<sub>4</sub>, and C<sub>2</sub>H<sub>6</sub>.<sup>[5]</sup> Kriston et al. performed simultaneous thermal analysis (STA) with GC/MS and FTIR for graphite anodes and Li<sub>x</sub>Ni<sub>1/3</sub>Mn<sub>1/3</sub>Co<sub>1/3</sub>O<sub>2</sub> cathodes.<sup>[6]</sup> Their results suggested that thermal decomposition happens in series of chain reactions that run out of control resulting in fires or explosions.<sup>[6]</sup> Our group recently investigated the thermal behavior of unaged and aged commercial 18650 cells using ARC and STA for the cell and material levels,<sup>[7–9]</sup> respectively. Stenzel et al. investigated graphite anodes and NMC622 cathodes at different SOCs by DSC, TGA, EGA-MS, and pyrolysis-GC-MS. The thermal decomposition products of SEI and CEI are depending on the SOC.<sup>[10]</sup>

Cycling at low temperatures, fast-charging, and overcharge can lead to negative anode potentials vs. Li/Li<sup>+</sup> where Li deposition on the anode gets thermodynamically

[a] Dr. A. A. Abd-El-Latif, P. Sichler, M. Kasper, Dr. T. Waldmann, Dr. M. Wohlfahrt-Mehrens  
ZSW – Zentrum für Sonnenenergie- und Wasserstoff-Forschung Baden-Württemberg  
Helmholtzstrasse 8, 89081 Ulm, Germany  
Fax: (+49) 731-9530-666  
E-mail: thomas.waldmann@zsw-bw.de

An invited contribution to a joint Special Collection between Batteries & Supercaps and Chemistry-Methods on In Situ and Operando Methods for Energy Storage and Conversion

© 2021 The Authors. *Batteries & Supercaps* published by Wiley-VCH GmbH. This is an open access article under the terms of the Creative Commons Attribution License, which permits use, distribution and reproduction in any medium, provided the original work is properly cited.

allowed.<sup>[11,12,13]</sup> Due to the high surface area of deposited Li and reactivity with electrolyte, Li-ion cells with this severe aging mechanism show an onset of exothermic reactions at 35 °C under the quasi-adiabatic conditions of ARC tests.<sup>[8,9]</sup> The effect of cathode active materials on safety behavior and on the evolved gases has been studied by Golubkov et al.<sup>[14]</sup> A huge amount of gases were formed in NCA cells compared with LFP cells and the thermal runaway is depending on the SOC.<sup>[15]</sup>

Internal and external pressure changes during ARC tests of commercial 18650-type LIBs were investigated in Seifert's group<sup>[16]</sup> The internal pressure rises until it falls after venting of the cell, followed by a steep increase of pressure outside of the cells during the explosion.<sup>[16]</sup>

To the best of our knowledge, there are no studies available on simultaneous gas analysis during ARC thermal runaway experiments, although information on evolving gases are highly relevant for safety evaluation. Mass spectrometry has become an indispensable analytical technique for the qualitative and quantitative detection of volatile reactants and products that are formed during the electrochemical reactions e.g., in fuel cells,<sup>[17]</sup> metal-ion batteries,<sup>[18]</sup> and metal-air batteries.<sup>[19]</sup>

In the present work, we developed a new method to study the evolving gases during venting and thermal runaway online. This is achieved by coupling an online MS<sup>[20]</sup> with the surrounding of the ARC instrument. Extra sensors for audio, humidity, and gases were applied for additional data collection. A comparison between the detected gases and thermal data of unaged, aged, and overcharged cells will be discussed in this article in addition to the expected decomposition reactions and their sequence.

## Experimental Section

The studied commercial 18650-type graphite/LiNi<sub>0.80</sub>Co<sub>0.15</sub>Al<sub>0.05</sub>O<sub>2</sub> cells have a specified voltage range of 2.5–4.2 V and a specific capacity of 3.25 Ah. All electrochemical tests were conducted with a Basytec CTS and climate chambers (Vötsch). All ARC tests were carried out with fully charged cells (CC-CV charging at 0.5 C to 4.2 V, the CV phase was cancelled when  $I < 0.05C$ ).

The following three types of ARC experiments were considered:

- 1) Heat-wait-seek experiment with unaged cells. These experiments serve as a baseline for comparison with the aged and overcharged cells.
- 2) Heat-wait-seek experiment with aged cells: Aging of the cells was performed by cycling them 18 times with a rate of 0.5 C at an ambient temperature of 0 °C.
- 3) Overcharge in ARC with unaged cells: The cells were overcharged inside the ARC with a rate of 0.5 C. It is noted that the heat produced by the overcharge leads to a change to the exothermal mode of the ARC.

All tested cells are fully charged directly with a short rest time (< 2 h) before the experiments, since rest times can change the result.<sup>[8]</sup> All ARC experiments were performed with two cells.

Figure 1 illustrates the newly developed combination between ARC and online gas analysis by MS and the positions of the additional sensors in this work. The details of the ARC experiment were published previously.<sup>[8,9]</sup> In brief, an ARC-EV, manufactured by Thermal Hazard Technology (THT, UK) was used. An N-type

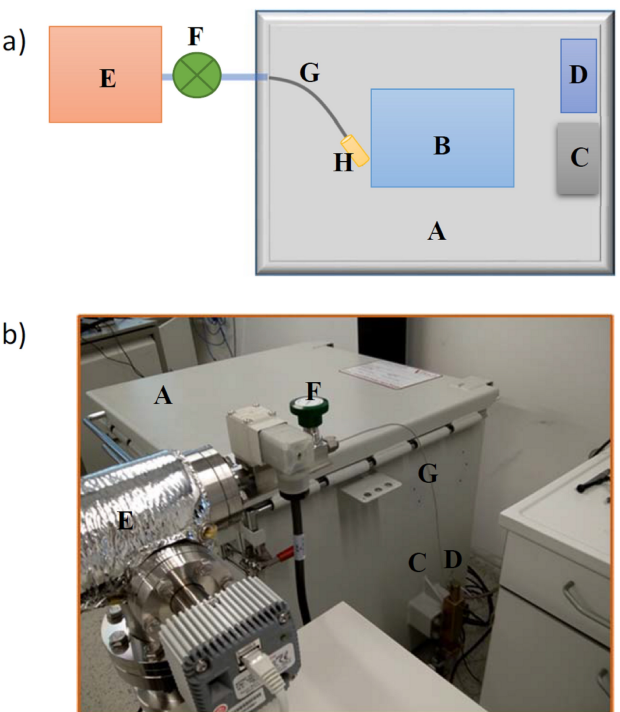


**Figure 1.** a) Illustration of ARC coupled with MS and different sensors. A: blast box, B: calorimeter containing the cell, C: audio recorder, D: additional sensors, E: MS, F: connecting valve, G: metal capillary, and H: Teflon membrane. b) Photograph of the ARC-MS setup from outside.

thermocouple was mounted on the cell body at half height to monitor the temperature of the 18650 cells during the ARC experiments. Before running the ARC experiment, the device was calibrated until a drift limit  $< 0.01\text{ }^{\circ}\text{C}/\text{min}$ . All experiments were conducted with an initial temperature of 35 °C. The temperature was increased in steps of 5 °C followed by a waiting period of 15 min and a seek period of 10 min. The cell temperature was followed if the self-heating rate surpassed  $0.02\text{ }^{\circ}\text{C}\text{min}^{-1}$  during the seek-period. The temperature of the thermal runaway was estimated at the intercept of the tangents before and after an abrupt rise in the temperature curve.

In order to investigate the effect of aging and overcharging of the commercial cell on the type and amount of emitted gases during venting and explosion, a MS (HPR40, HIDEN Analytical, UK) was connected to the ARC system via a metal capillary tube (G in Figure 1) and a Swagelok valve (F in Figure 1). Two layers of 20 nm pore size Teflon membrane (PF-002H, Hangzhou Cobetter Filtration Equipment Co., LTD, China, H in Figure 1) were fixed at the capillary end inside the blast box to avoid the diffusion of dust and organic electrolyte through the capillary into the vacuum system of MS. We note that the MS detects the gases in contact with air released from the cell. Before starting the experiment, the valve was stepwise opened until the pressure of the vacuum system and inside the capillary reached  $10^{-6}$  mbar then the ARC experiment was started and the ionic signals were simultaneously recorded. Hydrogen ( $m/z=2$ ), ethylene ( $m/z=26, 27$  and  $28$ ), CO<sub>2</sub> ( $m/z=22$  and  $44$ ), oxygen ( $m/z=32$ ), argon ( $m/z=40$ ), EMC ( $I_{45}, I_{59}$  and  $I_{90}$  which have a relative intensity of 0.65, 0.2 and 0.1 of the main peak at  $m/z=29$  respectively), DMC ( $I_{45}$  is the main peak and  $I_{59}=0.75$  of the main peak) and POF<sub>3</sub> ( $I_{104}$  is the main peak,  $I_{85}$  and  $I_{69}$  have a relative intensity of 85% and 20% respectively) were monitored.

A portable audio recorder (TASCAM DR-05, 44.1 kHz, mp3, 32 kbit/s, mono, C in Figure 1), kept in a filter bag (Kärcher 6.904-329.0) to keep it free from dust and located inside the blast box, was used to record the noise of the thermal runaway for the tested cell. A description of audio data analysis was published previously.<sup>[9]</sup>

A group of sensors, (PPD42NS, Grove-Dust sensor,  $>1\text{ }\mu\text{m}$ , Reichelt, D in Figure 1) (TGS-822 sensor for organic solvent and CO, Figaro) (TGS2600 sensor for  $\text{CH}_4$ , CO,  $\text{H}_2$  and ethanol, Figaro) (AS-MLC sensor for CO, AppliedSensor) (Z2000 - Humidity sensor, Hioki) (MB GAS-SENS V1 sensor for  $\text{H}_2$ , alcohol,  $\text{C}_1\text{-}\text{C}_4$  alkane, reichelt) were fixed in one corner of the ARC blast box and the signals were collected by a Hioki data logger (LR 8400-20) additionally to the MS signals. The principle of the dust sensor is that particles go through a light barrier and therefore reduce the signal. Therefore, a decreasing dust signal must be interpreted as high dust amount.

In order to analyze the electrolyte of the unaged cell, it was opened inside the glovebox under Ar atmosphere. Pieces of anode, cathode, and separators were cut and separately saved in vials for headspace GC/MS (Clarus 680/600T gas chromatograph/mass spectrometer (Perkin Elmer) with flame ionization detector) analysis. A type HS40 autosampler from Perkin Elmer was used for headspace injection. The autosampler was connected directly to the injector of the gas chromatograph via a deactivated silica transfer capillary. A medium polar Elite-624 was used as the separation column: 94% dimethylpolysiloxane, 6% cyclopropyl-phenyl residues, 60 m length, 0.32 mm internal diameter and the temperature program was chosen between 50–200°C with a rate of 10°C / min, then the temperature was held at 200°C for 15 min.

## 2. Results and Discussion

### 2.1. Thermal Behavior

Figure 2 shows the temperature evolution for the unaged, aged, and overcharged cells during the ARC experiments. The

curve shapes and maxima show a reasonable reproducibility. The steep temperature rise indicating the thermal runaway is obvious in all curves. Venting of the cells is indicated by a temperature drop as shown by the inset in Figure 2. The maximum temperatures are in the range of 714–868°C which is in agreement with the range observed earlier with similar cells.<sup>[9]</sup> The overcharged cells show the earliest thermal runaway. We note that this is connected to the energy which is actively charged into the cell during the experiment. During the overcharge, the cells heat up mainly due to their ohmic resistance.<sup>[21]</sup> This temperature rise is interpreted as exothermic reaction by the ARC device for the overcharged cells. Therefore the switching to the exothermic mode happens earliest for the overcharged cells. The thermal runaway happens after only two hours in this case. On the other hand, the unaged cells behave thermally most stable as expected. The temperature rise for the aged cell with Li deposition is located between the overcharged and the unaged cell.

As mentioned above, the ohmic resistance in combination with the charging current leads to an apparent  $T_{\text{SH}} = 35\text{ }^{\circ}\text{C}$  for the overcharged cells. This value is similar to the value of the aged cell and deposition of Li metal is likely the case in both cells.<sup>[8,9,22,23]</sup> The  $T_{\text{SH}}$  for unaged cell is around 96 °C.

All thermal parameters, i.e., onset-of-self-heating  $T_{\text{SH}}$ , venting  $T_{\text{vent}}$ , onset-of-thermal-runaway  $T_{\text{TR}}$  and maximum temperature  $T_{\text{max}}$  of the studied cells are summarized in Table 1. The venting takes place at  $\sim 123\text{ }^{\circ}\text{C}$ ,  $\sim 115\text{ }^{\circ}\text{C}$ , and  $\sim 135\text{ }^{\circ}\text{C}$  for overcharged, aged and unaged cells, respectively. However,  $T_{\text{TR}}$  of the overcharged cell is  $\sim 149\text{ }^{\circ}\text{C}$  which is significantly lower compared to the value for the unaged and aged cells ( $\sim 190\text{ }^{\circ}\text{C}$ ). The same trend can be seen in the temperature rise (Figure 2). The difference might be explained by the higher charged

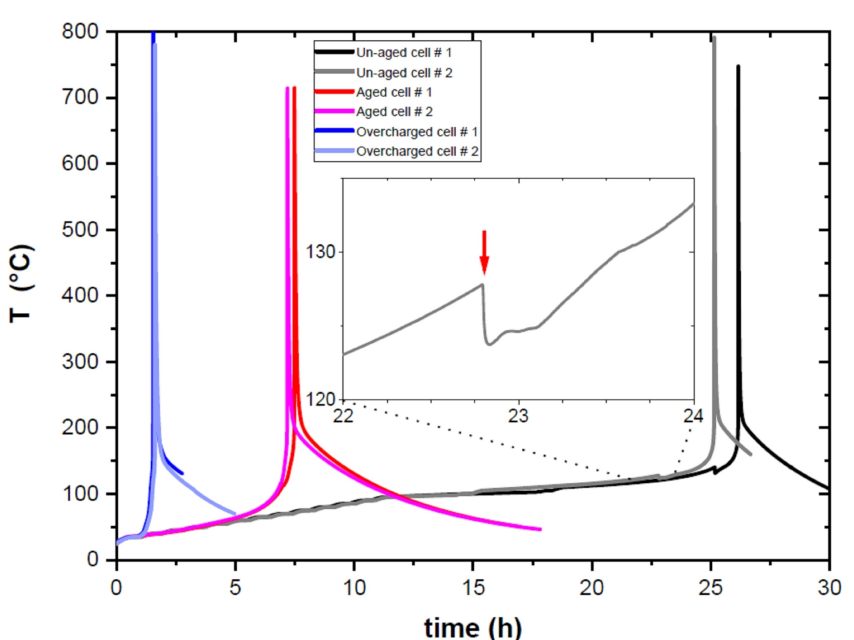


Figure 2. Comparison between the accelerating rate calorimetry data for unaged, aged, and overcharged commercial 18650 lithium-ion batteries. The arrow in the inset marks the venting temperature.

Thermal parameters	Unaged cell		Aged cell		Overcharged cell	
	# 1	# 2	# 1	# 2	# 1	# 2
$T_{SH}$ [°C]	96	96	36	36	35	35
$T_{vent}$ [°C]	141	128	114	116	123	123
$T_{TR}$ [°C]	194	194	188	189	150	149
$T_{max}$ [°C]	747	791	715	714	868	780

capacity and therefore in the higher reactivity of the materials in the overcharged cell.

Evaluation of the thermal data from Figure 2 yields only limited information about the cell characteristics such as venting which was determined from the temperature drop and is weakly pronounced in some cases. Furthermore, from these measurements no information on evolving gases is obtained. Therefore, in the following we analyze these cells with online gas analysis and additional external sensors.

## 2.2. Gas Evolution During ARC Tests

### 2.2.1. Unaged Cells

Figure 3 shows the thermal runaway analysis of a completely charged unaged 18650-type cell and the simultaneously recorded internal resistance, cell voltage, mass spectrometric ionic currents for gaseous ethylene,  $\text{CO}_2$ , organic solvents (DMC/EMC), and  $\text{POF}_3$  in addition to the signals of the gas sensors, dust, humidity, and the audio recorder. These simultaneously recorded values allow drawing further conclusions on the processes in the cell.

The cell resistance  $R$  increases gradually for ~20 hours followed by an abrupt increase at 112 °C before cell venting (Figure 3f). The resistance increase is accompanied by a sudden drop of the cell voltage. Therefore, these features most likely indicate the closing of the separator pores. However, we note that the voltage is changing afterwards again (see below).

Venting of the unaged cells is indicated by a drop in the temperature after ~25 h at ~141 °C (see inset of Figure 3a and Table 1). This temperature drop coincides with the voltage rise (Figure 3f), an increase of dust (Figure 3e), increased audio level (inset in Figure 3b), as well as increasing signals in the MS (Figure 3b,c) and the gas sensors (Figure 3d) in the blast box. The drop in temperature can therefore be explained by evaporation of electrolyte after cell venting.

The thermal runaway happens for the unaged cell approximately 50 min after the venting, as indicated by a steep increase of temperature. The temperature increase coincides with additional peaks for dust (Figure 3e) and increased audio level (inset in Figure 3c), as well as MS (Figure 3b,c) and sensor (Figure 3d) signals due to the explosion of the cell. As expected, the cell voltage drops to 0 V afterward (Figure 3f). It is noted that the audio levels of the venting were lower by approximately one order of magnitude in all cases compared to the

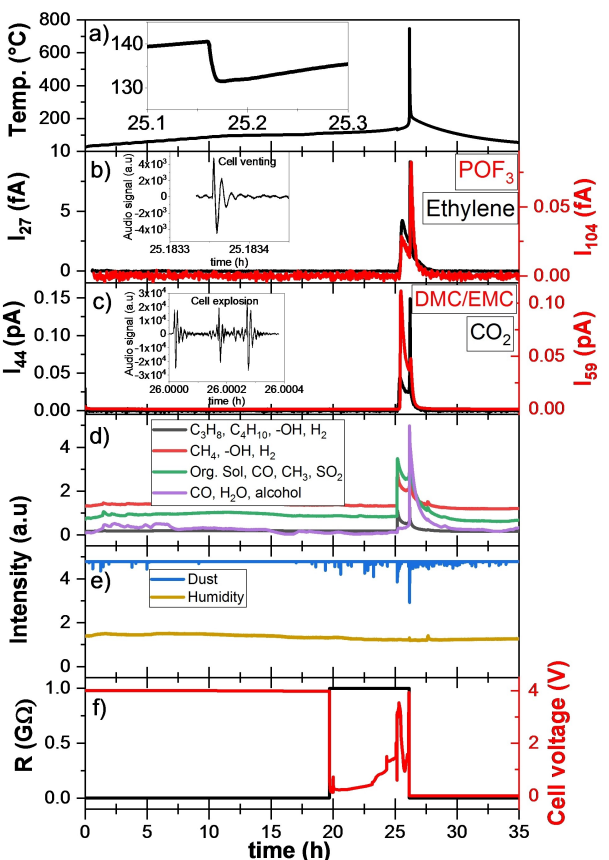
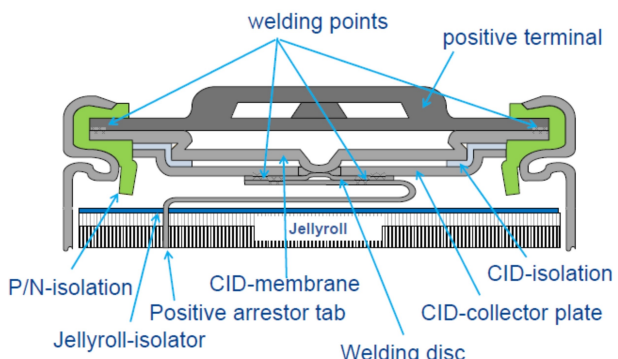


Figure 3. Simultaneously recorded thermal analysis of an unaged 18650 cylindrical cell by ARC (a) and the corresponding internal resistance and cell voltage (f), sensor signals (d, e), and mass spectrometric ionic current for  $m/z$ : 44 ( $\text{CO}_2$ ), 27 ( $\text{CH}_2=\text{CH}_2$ ), 59 (DMC/EMC), and 104 ( $\text{POF}_3$ ) (b, c). The inset in (a) shows the temperature drop due to venting. Insets in (b) and (c) are audio signals of cell venting and cell explosion, respectively. Higher dust amounts in (e) are indicated by lower sensor values.

explosion noise. Both can also be clearly distinguished by hearing their sound.

It is further noted that the internal resistance drops also to a very low value after the cell explosion, which is not the case for all cells (see, e.g., Figure 7f). Therefore, in the experiment shown in Figure 3f, most likely a short circuit occurred for specific parts of the cells which were connected to the ohmmeter or is due to the melting of positive/negative (P/N) isolation (330 °C for polyimide)<sup>[24]</sup> as shown in Figure 4. Such short-circuiting behavior is likely to have consequences for battery packs when a single cell therein shows a thermal runaway. In the case of a serial connection (e.g. 4s1p), this will lower the voltage of the parallel connected section. If the cell is parallel connected to other cells (e.g. 1s4p), this will short circuit the other cells and could therefore lead to an 'electrical propagation' of thermal runaway even if the cells are thermally well isolated.

The MS ionic currents for gases in the surrounding of the cell (inside the blast box) are shown in Figure 3b,c. Before the cell venting, there is no change in the intensity of the baselines of the whole detected fragments. The ionic currents start to increase simultaneously with the cell venting producing peaks



**Figure 4.** Cross-section drawing for the upper components of the cylindrical cells.

for gaseous ethylene,  $\text{CO}_2$ , EMC/DMC, and  $\text{POF}_3$  followed later by sharp spikes resulting from a high amount of gas formation during the cell explosion. The intensity of the organic solvent peak ( $m/z=59$ ) shows a high response corresponding to a huge amount of solvent vapor emitted during cell venting at  $141^\circ\text{C}$ . From Post-Mortem analysis of the unaged cell, we know that EMC/DMC is a part of the electrolyte (see Figure 5) in addition to EC and MPC (methyl phenyl carbonate). However, the other gases must have thermally evolved during the ARC experiment. The organic solvent signals are predominant at the time of cell venting whereas the  $\text{CO}_2$  signal is more prevailing later at cell explosion. The possible mechanism of gas evolution is discussed in detail in section 2.3.2. It is further noted that the humidity inside the blast box does mostly not change during the experiment (Figure 3e), indicating that no large amounts of water are created or consumed.

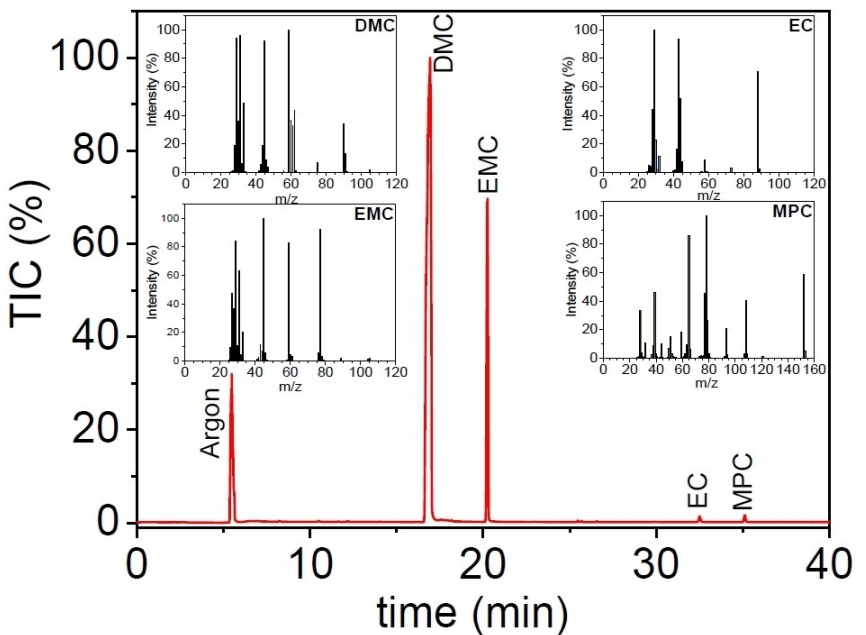
Comparing the signals for the gas sensors (Figure 3d) with the MS measurement (Figure 3b,c), signals occur at the same time for both methods. However, it is important to mention that the gas sensors do not react on specific gases. Therefore, it is not possible to compare the type of gases or the intensities by the gas sensors at the moment. A qualitative evaluation or detection of specific gases is only possible by the MS method. However, the sensors might be useful as a low-cost solution for the detection of cell leakage in applications.

### 2.2.2. Aged Cell with Li Deposition

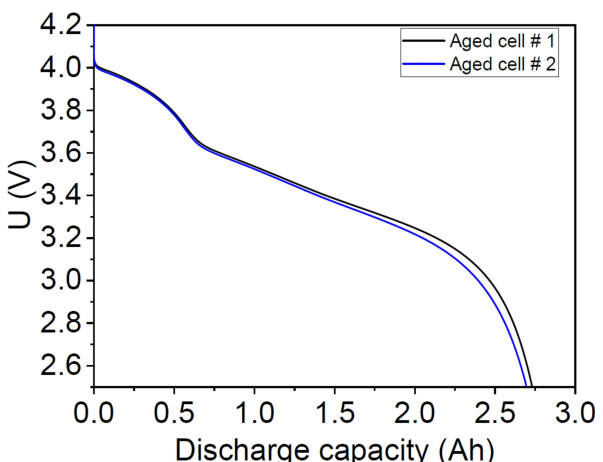
Figure 6 shows the voltage-discharge capacity curves of the first cycle for the aged cells at  $0^\circ\text{C}$ . The voltage plateau between 0Ah and 0.5Ah was attributed in literature to the stripping of previously deposited lithium on anode during the charging at  $0^\circ\text{C}$ .<sup>[9,25]</sup>

Figure 7 shows the thermal runaway analysis of an aged cell which was analogously plotted as for the unaged cell in Figure 3. The results of Figure 7 show the higher reactivity of the aged cell in comparison with an unaged cell. The self-heating process starts early after 50 min at  $36^\circ\text{C}$  and the  $T_{\text{TR}}$  is  $188^\circ\text{C}$  after 7.5 hours, which is close to the melting point of Li metal ( $180.5^\circ\text{C}$ ). We had reported earlier on similar values for cells with Li deposition for other cell types.<sup>[7–9]</sup>

The cell resistance increased gradually for 6.5 hours followed by a sudden increase at  $88^\circ\text{C}$  before cell venting which takes place at  $114^\circ\text{C}$  after approximately 7 hours as shown in Figure 7a. After venting, air might intrude into the cell and react with the cell components. Since deposited Li metal on the graphite anode is known to react with  $\text{H}_2\text{O}$ , it is interesting to compare the levels of humidity inside the blast



**Figure 5.** GC/MS analysis for the electrolyte of an opened unaged cylindrical cell (post-mortem analysis). Insets: Recorded mass spectra for the detected species.



**Figure 6.** Cell voltage vs. discharge capacity profile of aged cells at 0.5 C of the first discharge after charging at 0 °C. The voltage plateau indicates stripping of previously deposited Li from the anode.

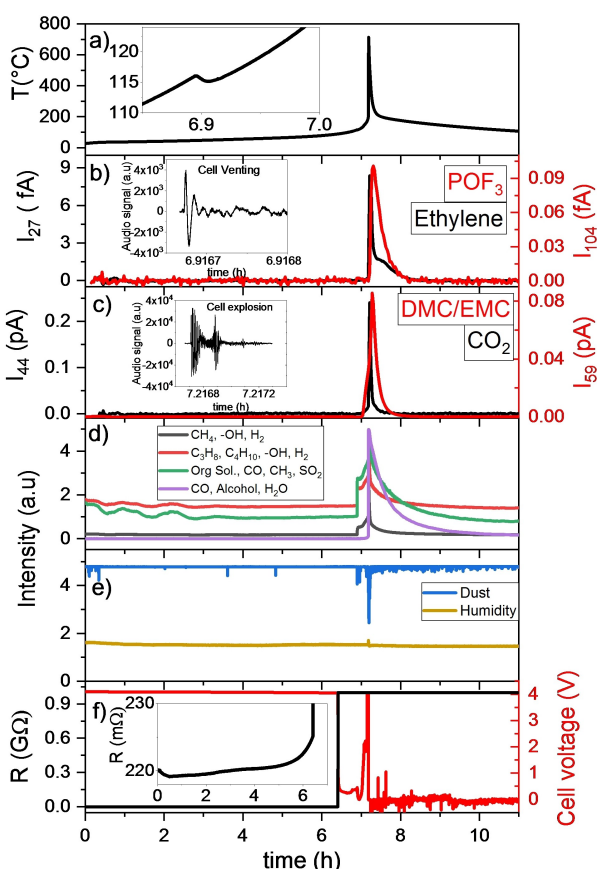


**Figure 7.** Simultaneously recorded thermal analysis of an aged 18650 cylindrical cell by ARC (a) and the corresponding internal resistance and cell voltage (f), sensor signals (d, e), and mass spectrometric ionic current for  $m/z$ : 44 ( $\text{CO}_2$ ), 27 ( $\text{CH}_4 = \text{CH}_2$ ), 59 (DMC/EMC), and 104 ( $\text{POF}_3$ ) (b, c). The inset in (a) shows the temperature drop due to venting. Insets in (b) and (c) are audio signals of cell venting and cell explosion, respectively. Higher dust amounts in (e) are indicated by lower sensor values.

box in the experiments of the unaged and the aged cells. In fact, the humidity was on similar levels in the experiments with

the unaged (Figure 3e) and aged cell (Figure 7e). Nevertheless, the reaction is much faster for the aged cell. Therefore, the intruding humidity and reaction with deposited Li metal is most likely not the main cause for the higher reactivity of the aged cell. It is more likely that the faster reaction the ARC experiment is due to reaction of Li metal with electrolyte and the excess of the melting point of Li (180.5 °C).

The cell voltage suddenly decreased before cell venting, simultaneously with the huge rise in the cell resistance (Figure 7f). The reason could be the accumulation of the formed gases and consequently the separation of anode and cathode as observed by Finegan et al.<sup>[26]</sup> Afterwards, the cell voltage fluctuates and reaches the maximum value (4.2 V) at the cell explosion before to reach 0 V.

Differently than the results of the unaged cells, only one high ionic current peak is observed for  $\text{C}_2\text{H}_4$ ,  $\text{CO}_2$ ,  $\text{POF}_3$ , and DMC/EMC (Figure 7b,c). This single (superimposed) peak is due to the short time difference between the cell venting and the cell explosion. It is obvious that the broad peak of organic vapor results from the overlapping between two peaks corresponding to the two thermal processes of venting and explosion of the aged cell. The signals of the gas sensors again confirm the emission of gases during venting and explosion. The gas sensors (Figure 7d) also show the trend of shorter time between venting and thermal runaway for the aged cell like the MS results.

In contrast, the audio signals for venting and explosion (insets of Figure 7b,c) show that both processes are not occurring at the same time, however, with a time difference of ~0.3 h. This is also consistent two separate peaks from the dust sensor (Figure 7e). The resolution of the dust and audio sensors is therefore valuable to distinguish between both processes.

### 2.2.3. Overcharged Cells

Figure 8a shows the increase of temperature in an overcharge experiment of an unaged cell in the ARC. After 50 min, the cell voltage started to increase gradually to 5.1 V for ~30 min then the voltage decays linearly to 4.9 V within 5 minutes (decreasing rate  $< 1 \text{ mV/s}$ ). The thermal runaway of this cell was initiated at 149 °C, which is the lowest  $T_{TR}$  of the studied cells. For overcharging it is known that the anode potential can get in a critically low range.<sup>[27]</sup> Therefore, overcharging can lead to Li deposition similarly to the aged cell cycled at low temperature.<sup>[28]</sup>

A current drop is observed approximately 3 min before the venting. One reason for the current interruption could be an internal short circuit due to Li dendrites<sup>[28]</sup> growing from anode to cathode due to overcharge. However, since the current interruption coincides with the cell venting, it is more likely that breaking of the CID (Figure 4) due to high internal gas pressure has interrupted the charging current.

After the current interruption, the temperature of the cell is spontaneously increasing until reaching the cell explosion after ~90 min from the beginning of experiment. The mass spectrometric ionic signals show the parallel onset of  $\text{CO}_2$ ,  $\text{C}_2\text{H}_4$ , and

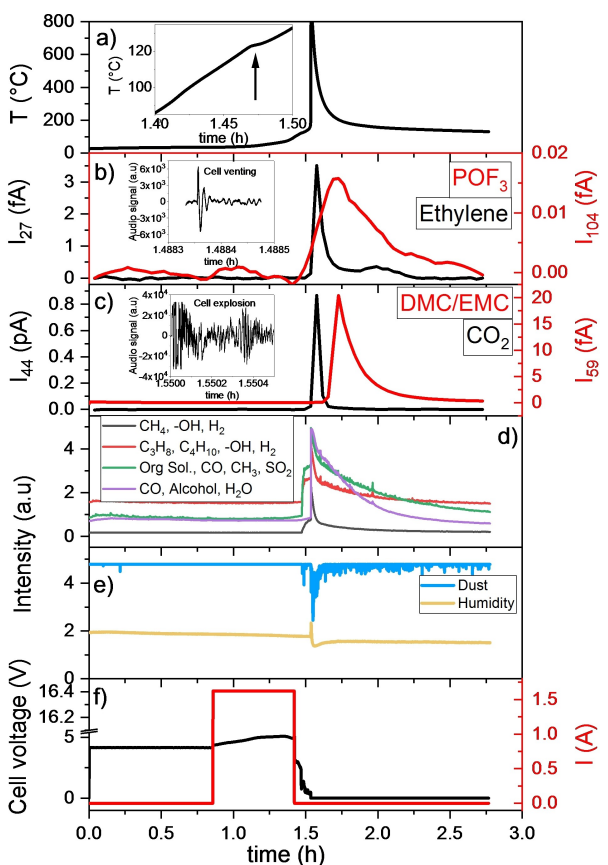


**Figure 8.** Simultaneously recorded thermal analysis of an overcharged 18650 cylindrical cell by ARC (a) and the corresponding cell voltage and current (f), sensor signals (d, e), and mass spectrometric ionic current for  $m/z$ : 44 ( $\text{CO}_2$ ), 27 ( $\text{CH}_2=\text{CH}_2$ ), 59 (DMC/EMC), and 104 ( $\text{POF}_3$ ) (b, c). The inset in (a) shows the temperature slope change due to venting. Insets in (b) and (c) are audio signals of cell venting and cell explosion, respectively. We note that the overcharging program started 50 min after stabilizing the baseline of ionic signals. Higher dust amounts in (e) are indicated by lower sensor values.

$\text{POF}_3$  emission to the cell explosion peak (Figure 8b,c). In spite of the late detection of the DMC/EMC signal, the decay of  $\text{POF}_3$  and vapor of DMC/EMC is elongated. Similarly to the non-overcharged cells, the change of the gas sensor signals are detectable. The onset of the gas sensors signals start in parallel to the increase of ionic current for the detected fragments by MS and by the drop in the current and cell voltage.

It is noted that the humidity signal is changing during the explosion of the overcharged cell, indicating a possible cross-sensitivity of this sensor (Figure 8e). In fact, this can also be seen in a much weaker form in Figure 3 and Figure 7, indicating that the amount emitted gases within a short time is likely much stronger for the overcharged cell. A similar trend is shown by the dust sensor (Figure 8e), which shows a clearer increase in the case of the overcharged cells compared to the unaged and aged cells.

The overcharged cell showed the highest reactivity in comparison with the other tests in this work which is connected to SOC > 100%. This is in agreement with experiments of other cell types with NCA cathode for which the order

of stability was reported to be discharged > partially charged > fully charged > overcharged.<sup>[15]</sup>

### 2.3. Comparison Between the Tested Cells

#### 2.3.1. Amount of Evolved Gases

Figure 9 and Table 2 show the recorded intensities for ethylene,  $\text{CO}_2$ ,  $\text{POF}_3$ , and  $m/z=45$  (DMC/EMC) (the related ionic signal is not shown in Figures 3, 7 and 8, however, the integrated charge is reported in Table 2) and  $m/z=59$  (DMC/EMC). The integrated ionic charge data show that approximately the double amount of solvent is evaporating from the unaged cell compared with the aged cell. The same ratio was obtained for ethylene and  $\text{CO}_2$ . This decay in the amount of the emitted gas might be consumed during the aging process of the cell. The order of the evolved amount of gases from the studied cells follow mostly (except  $\text{CO}_2$ ) the same order of the time period between the cell venting and explosion. The long period at high temperature during the ARC experiment in case of unaged cell is likely enough to accumulate a high amount of gases before cell explosion. In contrast, the  $\text{CO}_2$  amount is approximately the same for the unaged and for the overcharged cells, indicating a different mechanism in both cases. The gas formation mechanism will be discussed in the next section.

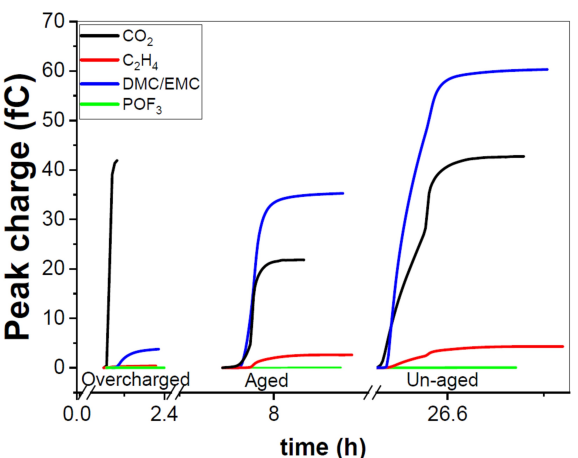


**Figure 9.** Comparison between the integrated ionic charges of the gases evolved from the unaged, aged and overcharged cells during the thermal runaway.

**Table 2.** Integrated charge values (in Coulomb) of the evolved gases during the ARC experiment for unaged, aged cell and overcharged cell.

Detected gas	Unaged cell		Aged cell		Overcharged cell	
	# 1	# 2	# 1	# 2	# 1	# 2
$m/z=27(\text{C}_2\text{H}_4)/10^{-15}$	4.3	5.1	2.6	1.6	0.4	0.2
$m/z=44(\text{CO}_2)/10^{-15}$	43.0	63.5	22.0	18.0	42.0	26.6
$m/z=45(\text{DMC/EMC})/10^{-15}$	140.0	180.0	75.3	43.2	10.0	9.1
$m/z=59(\text{DMC/EMC})/10^{-15}$	60.0	83.0	35.0	20.0	3.8	2.9
$m/z=85(\text{POF}_3)/10^{-17}$	4.10	3.8	3.44	3.30	0.7	0.4

### 2.3.2. Mechanism of Gas Formation

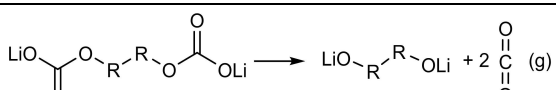
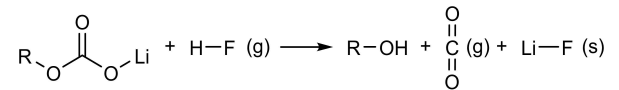
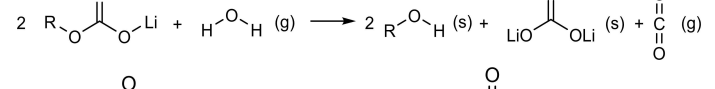
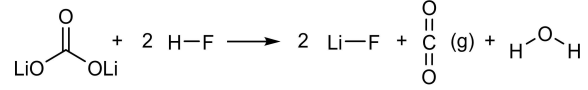
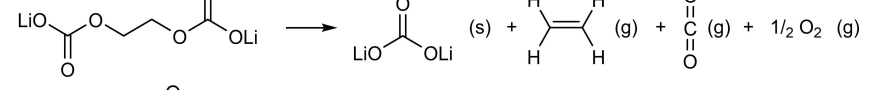
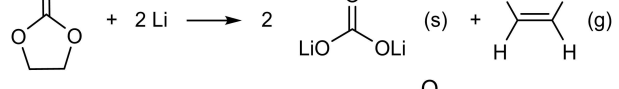
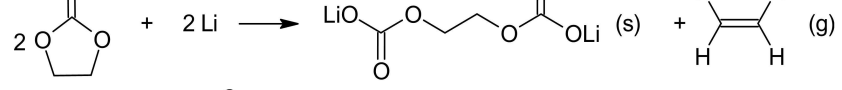
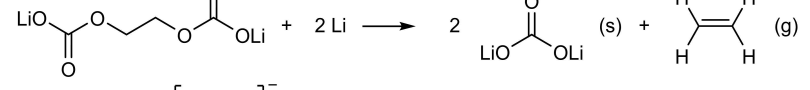
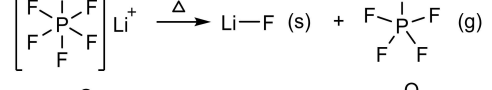
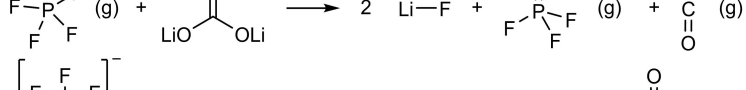
The qualitative and semi-quantitative gas analysis was performed during the thermal runaway of unaged, aged, and overcharged lithium-ion batteries depending on the mass spectrometric signal intensities. The thermal decomposition profile of the cells can be divided into three regions according to main peaks of gas emission:

- 1) In the first region before cell venting, at 125°C for unaged and overcharged cells and at 114°C for the aged cells, no gas formation is detected outside of the cells.
- 2) In the second region directly after cell venting, the main emitted gases from unaged cells are organic solvent vapors due to their low boiling points of 90°C (DMC) and 107°C (EMC), and minor signals of CO<sub>2</sub>, CH<sub>2</sub>=CH<sub>2</sub>, and POF<sub>3</sub> as seen in the mass spectrometric signals.

- 3) In the third region during cell explosion, the predominant gas products ethylene, carbon dioxide, and POF<sub>3</sub> are detected for all experiments.

It is worth noting that the separation of the ionic peaks corresponding to the cell venting and thermal runaway is very clear for the unaged cell. On another hand, the peak separation disappeared for the aged and overcharged cells resulting from their deteriorated thermal stability and accelerated degradation. The main reason for earlier thermal runaway of lithium ion batteries is Li deposition which can be formed by overcharging, fast charging or charging at low temperature.<sup>[13,23,28,29]</sup> Li deposition is present in the case of the aged cells and as well as most likely in the overcharged cells. Li deposition on anodes becomes thermodynamically possible when the anode potentials gets negative vs. Li/Li<sup>+</sup><sup>[30]</sup> and it becomes generally more severe if cells are cycled at low temperatures.<sup>[12]</sup>

**Table 3.** Suggested gas evolution reactions during thermal runaway.

Evolved gas	Chemical reactions	No.
CO <sub>2</sub>		1
		2
		3
CO <sub>2</sub> and C <sub>2</sub> H <sub>4</sub>		4
		5
C <sub>2</sub> H <sub>4</sub>		6
		7
POF <sub>3</sub>		8
		9
		10
		11

The evolved gases during the thermal runaway are driven by thermally and electrochemically reactions of the electrolyte, electrode active materials, the SEI, binder, separator and the intercalated Li. Initial decomposition of the metastable SEI components occurs early to produce CO<sub>2</sub> and ethylene gases according to the following suggested reactions (1–3,5,8, Table 3).<sup>[14,31]</sup>

CO<sub>2</sub> might be also formed by the reaction of Li<sub>2</sub>CO<sub>3</sub>, which is produced by reduction of ethylene carbonate at the anode, with traces of HF according to reaction 4.

At the lithiated anode, ethylene carbonate will be reduced to ethylene gas, as shown in reactions 6 and 7<sup>[3,4,32]</sup> or by the decomposition of SEI (reaction 8).<sup>[33]</sup> However the thermal decomposition of dry LiPF<sub>6</sub> takes place between 100°C and 200°C,<sup>[34]</sup> at room temperature LiPF<sub>6</sub> decomposition will be initiated by oxygen containing species such as H<sub>2</sub>O or Li<sub>2</sub>CO<sub>3</sub> according to reactions 9–11.<sup>[35]</sup>

### 3. Conclusions

A new analytical method (ARC-MS) has been developed for coupling on-line mass spectrometry (MS) plus several other sensors with an accelerating rate calorimetry (ARC) device. This novel setup was used to analyze the progress of thermal runaway in commercial 18650-type Li-ion cells. Coupling to the

MS and additional sensors allows a more detailed detection of volatile product species in the surrounding of the cells and other safety relevant events during venting and thermal runaway.

Figure 10 shows an overview of the results. The time until thermal runaway decreases in the order of unaged cells > aged cells (main mechanism: Li deposition) > overcharged cells under the quasi-adiabatic conditions of the ARC test. Venting of the cells is accompanied by a release of gases and dust. Analysis of audio signals is helpful to determine the times of venting and explosion of the cells precisely and independently from thermal data.

Cell resistance changes indicate closing of separator pores as well as in some cases short-circuiting by melting of the P/N isolation in the lid of the cell housing happening during thermal runaway. Such short-circuiting is likely to affect additional cells in a battery system. When additional cells would be short-circuited by the concerned cell, this could be regarded as an electrical propagation of thermal runaway.

The main volatile products of the studied cells are evaporated organic solvents (DMC, EMC) during the venting of the cell, especially for unaged cells. Different types of gaseous products such as ethylene, CO<sub>2</sub>, and POF<sub>3</sub> were found during the explosions and result from thermal and electrochemical side reactions of electrolyte decomposition.

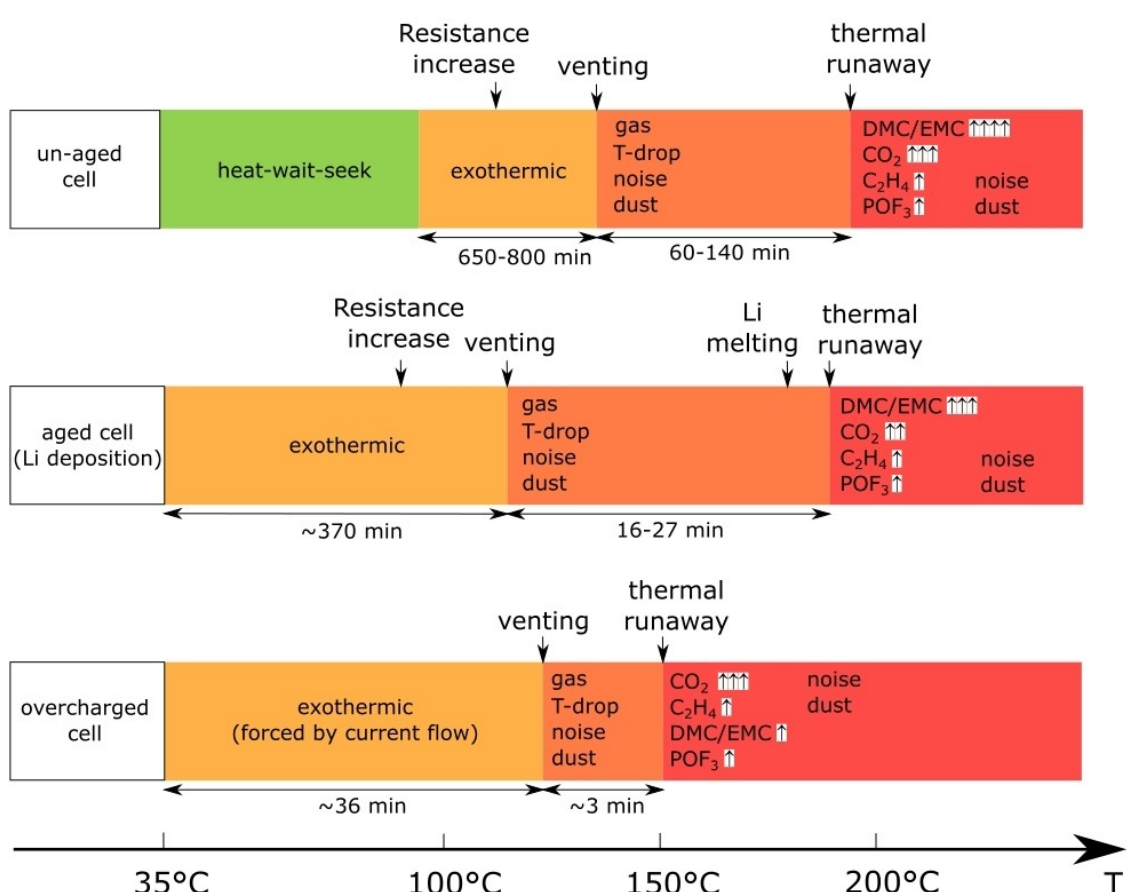


Figure 10. Overview on experimental results with ARC-MS.

We observed a temporal coincidence of the MS signals with those of additional gas sensors. Since leakage and venting correspond to hazard levels of 3 and 4 respectively,<sup>[36]</sup> an early detection by audio and gas sensors might be relevant as a low-cost solution for certain battery applications. However, for quantitative and specific detection of gases, the MS must be included in the experimental setup. The amount of released gases primarily depends on the history of the cells, i.e., if the cell is unaged, if the cell was cycled under Li deposition conditions as an aging mechanism, or if the cell is overcharged in the experiment.

ARC-MS is a novel and valuable tool to evaluate the thermal runaway behavior of LIBs including electrochemical, thermal, and gas evolution in air contact. Further studies in our lab are aiming on detecting the gases inside the cells without air contact.

## Acknowledgements

This research work has been performed within the TEESMAT project (<http://www.teesmat.eu>) and received funding from the European Community's Horizon 2020 Framework under Grant Agreement n° 814106. The authors would like to thank A. Aracil Regalado (ZSW) for performing the cell opening.

## Conflict of Interest

The authors declare no conflict of interest.

**Keywords:** lithium-ion cells · thermal runaway · online gas analysis · Li deposition · overcharge

- [1] a) T. Kodama, H. Sakaebe, *J. Power Sources* **1999**, *81*, 144–149; b) D. Deng, *Energy Sci Eng* **2015**, *3*, 385–418; c) N. Nitta, F. Wu, J. T. Lee, G. Yushin, *Mater. Today* **2015**, *18*, 252–264; d) A. Barré, B. Deguilhem, S. Grolleau, M. Gérard, F. Suard, D. Riu, *J. Power Sources* **2013**, *241*, 680–689.
- [2] a) D. Doughty, E. P. Roth, *Electrochim. Soc. Interface* **2012**, 37–44; b) X. Feng, M. Ouyang, X. Liu, L. Lu, Y. Xia, X. He, *Energy Storage Mater.* **2018**, *10*, 246–267; c) A. Hofmann, N. Uhlmann, C. Ziebert, O. Wiegand, A. Schmidt, T. Hanemann, *Appl. Therm. Eng.* **2017**, *124*, 539–544.
- [3] B. Liu, Y. Jia, C. Yuan, L. Wang, X. Gao, S. Yin, J. Xu, *Energy Storage Mater.* **2020**, *24*, 85–112.
- [4] E.P. Roth, D.H. Doughty, *J. Power Sources* **2004**, *128*, 308–318.
- [5] D.P. Abraham, E.P. Roth, R. Kostecki, K. McCarthy, S. MacLaren, D.H. Doughty, *J. Power Sources* **2006**, *161*, 648–657.
- [6] A. Kriston, I. Adanouj, V. Ruiz, A. Pfarrang, *J. Power Sources* **2019**, 435.
- [7] M. Fleischhammer, T. Waldmann, G. Bisle, B.-I. Hogg, M. Wohlfahrt-Mehrens, *J. Power Sources* **2015**, *274*, 432–439.
- [8] T. Waldmann, M. Wohlfahrt-Mehrens, *Electrochim. Acta* **2017**, *230*, 454–460.
- [9] T. Waldmann, J. B. Quinn, K. Richter, M. Kasper, A. Tost, A. Klein, M. Wohlfahrt-Mehrens, *J. Electrochim. Soc.* **2017**, *164*, A3154–A3162.
- [10] Y. P. Stenzel, M. Boerner, Y. Preibisch, M. Winter, S. Nowak, *J. Power Sources* **2019**, 433.
- [11] a) H.-p. Lin, D. Chua, M. Salomon, H.-C. Shiao, M. Hendrickson, E. Plichta, S. Slane, *Electrochim. Solid-State Lett.* **2001**, *4*, A71; b) T. Waldmann, M. Wilka, M. Kasper, M. Fleischhammer, M. Wohlfahrt-Mehrens, *J. Power Sources* **2014**, *262*, 129–135; c) T. Waldmann, B.-I. Hogg, M. Kasper, S.

- Grolleau, C. G. Couceiro, K. Trad, B. P. Matadi, M. Wohlfahrt-Mehrens, *J. Electrochim. Soc.* **2016**, *163*, A1232–A1238.
- [12] S. Hein, A. Latz, *Electrochim. Acta* **2016**, *201*, 354–365.
- [13] T. Waldmann, B.-I. Hogg, M. Wohlfahrt-Mehrens, *J. Power Sources* **2018**, *384*, 107–124.
- [14] A. W. Golubkov, D. Fuchs, J. Wagner, H. Wiltsche, C. Stangl, G. Fauler, G. Voitic, A. Thaler, V. Hacker, *RSC Adv.* **2014**, *4*, 3633–3642.
- [15] A. W. Golubkov, S. Scheikl, R. Planteu, G. Voitic, H. Wiltsche, C. Stangl, G. Fauler, A. Thaler, V. Hacker, *RSC Adv.* **2015**, *5*, 57171–57186.
- [16] B. Lei, W. Zhao, C. Ziebert, N. Uhlmann, M. Rohde, H. Seifert, *Batteries* **2017**, *3*, 14.
- [17] a) A. Abd-El-Latif, E. Mostafa, S. Huxter, G. Attard, H. Baltruschat, *Electrochim. Acta* **2010**, *55*, 7951–7960; b) A. A. Abd-El-Latif, H. Baltruschat, *J. Electroanal. Chem.* **2011**, *662*, 204–212; c) A. A. Abd-El-Latif, J. Xu, N. Bogolowski, P. Koenigshoven, H. Baltruschat, *Electrocatalysis* **2012**, *3*, 39–47.
- [18] a) J. Vetter, M. Holzapfel, A. Wuersig, W. Scheifele, J. Ufheil, P. Novák, *J. Power Sources* **2006**, *159*, 277–281; b) N. Tsiovaras, S. Meini, I. Buchberger, H. A. Gasteiger, *J. Electrochim. Soc.* **2013**, *160*, A471–A477; c) M. Metzger, C. Marino, J. Sicklinger, D. Haering, H. A. Gasteiger, *J. Electrochim. Soc.* **2015**, *162*, A1123–A1134.
- [19] a) P. Reinsberg, A. A. Abd-El-Latif, H. Baltruschat, *Electrochim. Acta* **2018**, *273*, 424–431; b) C. J. Bondue, P. Reinsberg, A. A. Abd-El-Latif, H. Baltruschat, *Phys. Chem. Chem. Phys.* **2015**, *17*, 25593–25606; c) C. J. Bondue, A. A. Abd-El-Latif, P. Hegemann, H. Baltruschat, *J. Electrochim. Soc.* **2015**, *162*, A479–A487; d) P. P. Bawol, P. Reinsberg, C. J. Bondue, A. A. Abd-El-Latif, P. Koenigshoven, H. Baltruschat, *Phys. Chem. Chem. Phys.* **2018**, *20*, 21447–21456.
- [20] A. A. Abd-El-Latif, C. J. Bondue, S. Ernst, M. Hegemann, J. K. Kaul, M. Khodayari, E. Mostafa, A. Stefanova, H. Baltruschat, *Trends Analyt. Chem.* **2015**, *70*, 4–13.
- [21] T. Waldmann, M. Kasper, M. Wohlfahrt-Mehrens, *Electrochim. Acta* **2015**, *178*, 525–532.
- [22] a) J. Liu, Q. Duan, M. Ma, C. Zhao, J. Sun, Q. Wang, *J. Power Sources* **2020**, *445*; b) W. Mei, L. Zhang, J. Sun, Q. Wang, *Energy Storage Mater.* **2020**, *32*, 91–104.
- [23] Q. Liu, C. Du, B. Shen, P. Zuo, X. Cheng, Y. Ma, G. Yin, Y. Gao, *RSC Adv.* **2016**, *6*, 88683–88700.
- [24] H. Zhang, W. Wang, G. Chen, A. Zhang, X. Fang, *Polymer* **2017**, *9*.
- [25] R. V. Bugga, M. C. Smart, *ECS Trans.* **2009**, *25*, 241–252.
- [26] D. P. Finegan et al., *Nat. Commun.* **2015**, *6*, 6924.
- [27] F. Grimsmann, T. Gerbert, F. Brauchle, A. Gruhle, J. Parisi, M. Knipper, *J. Energy Storage* **2018**, *15*, 17–22.
- [28] A. Tomaszewska et al., *eTransportation* **2019**, *1*, 100011.
- [29] a) D. Ren, X. Feng, L. Lu, X. He, M. Ouyang, *Appl. Energy* **2019**, *250*, 323–332; b) M. Ouyang, D. Ren, L. Lu, J. Li, X. Feng, X. Han, G. Liu, *J. Power Sources* **2015**, *279*, 626–635; c) D. Ren, K. Smith, D. Guo, X. Han, X. Feng, L. Lu, M. Ouyang, J. Li, *J. Electrochim. Soc.* **2018**, *165*, A2167–A2178; d) S. Ahmed et al., *J. Power Sources* **2017**, *367*, 250–262; e) Z. Li, J. Huang, B. Y. Liaw, V. Metzler, J. Zhang, *J. Power Sources* **2014**, *254*, 168–182; f) X. Han, L. Lu, Y. Zheng, X. Feng, Z. Li, J. Li, M. Ouyang, *eTransportation* **2019**, *1*, 100005.
- [30] H. Ge, T. Aoki, N. Ikeda, S. Suga, T. Isobe, Z. Li, Y. Tabuchi, J. Zhang, *J. Electrochim. Soc.* **2017**, *164*, A1050–A1060.
- [31] a) H. Yang, X.-D. Shen, *J. Power Sources* **2007**, *167*, 515–519; b) R. Spotnitz, J. Franklin, *J. Power Sources* **2003**, *113*, 81–100; c) M. N. Richard, J.R. Dahn, *J. Electrochim. Soc.* **1999**, *146*, 2078–2084; d) Q. S. Wang, J. H. Sun, X. L. Yao, C. H. Chen, *J. Electrochim. Soc.* **2006**, *153*, A329–A333.
- [32] Q. Wang, P. Ping, X. Zhao, G. Chu, J. Sun, C. Chen, *J. Power Sources* **2012**, *208*, 210–224.
- [33] M. N. Richard, J. R. Dahn, *J. Electrochim. Soc.* **1999**, *146*, 2068–2077.
- [34] a) H. Yang, G. V. Zhuang, Philip N. Ross Jr., *J. Power Sources* **2006**, *161*, 573–579; b) M. D. S. Lekgoathi, B. M. Vilakazi, J. B. Wagener, J. P. Le Roux, D. Moolman, *J. Fluorine Chem.* **2013**, *149*, 53–56.
- [35] V. Kraft, M. Gruetzeke, W. Weber, M. Winter, S. Nowak, *J. Chromatogr. A* **2014**, *1354*, 92–100.
- [36] C. Ashtiani, *ECS Trans.* **2007**, *11*, 1–11.

Manuscript received: January 26, 2021

Revised manuscript received: March 5, 2021

Version of record online: March 24, 2021